Preparation and enhanced photocatalytic performance of g-C_3N_4/TiO_2-SiO_2

W. CHANG[a,*], J. QIN[a], D. D. ZHENG[a], B. GAO[a], Y. F. LI[a], T. FUJINO[b]
[a]*College of Environmental and Chemical Engineering, Xi'an Polytechnic Universit y, Xi'an, 710048, China*
[b]*Department of applied chemistry, Toyo University, 2100 Kujirai, Kawagoe, Saitama, 350-8585, Japan*

The g-C_3N_4/TiO_2-SiO_2 was successfully prepared by sol gel method and calcination process. The samples were characterized by scanning electron microscopy, X ray diffraction and BET analysis etc. The results showed that the optimal amount doping of g-C_3N_4 with TiO_2-SiO_2 can improve the photocatalytic activity of the material. The enhanced photocatalytic activity can be ascribed to the beneficial microstructure and synergistic effects of g-C_3N_4 and TiO_2-SiO_2. The material can reduce the COD value of the actual wastewater effectively and it can also be recycled easily.

(Received August 7, 2020; accepted April 7, 2021)

Keywords: TiO_2-SiO_2, g-C_3N_4, Photocatalysis, Wastewater

1. Introduction

Water pollution and shortage of clean drinking water have raised widespread concerns these years. Especially, the dyeing wastewater containing a large amount of synthetic dyes poses a serious threat to the environment and consequently to human health [1-2]. The conventional wastewater treatment methods can only remove the pollutants from one phase to another phase or inadequately mineralize the organic pollutants, even leading to the secondary pollution [3-5]. Over the past few years, the photocatalytic oxidation technology has been proved to be an effective method for wastewater treatment. The photocatalytic degradation of organic pollutants is high efficiency, non-selective degradation and low cost. The photocatalytic activity of the photocatalysts is principally determined by its chemical and physical properties [6]. TiO_2 is widely used in photocatalytic processes such as self-cleaning air and water purification due to its chemistry stability, strong oxidation activity, nontoxicity and economic efficiency [7-9]. However, the relative wide band gap (3.2eV), the rapid recombination rate of photogenerated electron(e-)/hole pairs(h+) and difficult to recycle restricts its application in practice [10-13]. In our previous work, we found that doping SiO_2 and TiO_2 can increase the specific surface area, inhibit the transformation of anatase phase to rutile phase, adjust the band gap, and improve photocatalytic activity of the TiO_2 [14-15]. The TiO_2-SiO_2 can be prepared as monolithic material with rich pore structure and easy to be recycled.

The graphite carbon nitride (g-C_3N_4) is non-metallic semiconductor, composed of C and N elements which are abundant on the earth, with a band gap of about 2.7 eV. It is resistant to acid, alkali, and light corrosion, and has good stability [16-18]. The photocatalytic activity of g-C_3N_4 is not ideal due to its small specific surface area and fast electron-hole recombination rate [19,20]. Studies have shown that the structure and performance of g-C_3N_4 can be adjusted by physical modification, chemical doping, etc. It is reported that the chemical bond between the g-C_3N_4 and TiO_2 can form an effective channel for photogenerated electrons, which reduces the recombination rate of photogenerated electrons and holes and enhances the photocatalytic activity of g-C_3N_4 or TiO_2 [21-26]. The g-C_3N_4/TiO_2 can be prepared by hydrothermal [27], calcination [28, 29], microwave assisted method, etc. [30]. Therefore, in order to obtain the photocatalysts with enhanced photocatalytic activity, low cost and easy recovery, based on our previous work, g-C_3N_4/TiO_2-SiO_2 photocatalytic materials were prepared, and its characteristics and photocatalytic performance were studied. The results can provide a certain theoretical reference for the practical application of the prepared material.

2. Experimental

2.1. Preparation of materials

1 g PEG (Mr 20000) was dissolved in the solution with 2 mL furfuryl alcohol, 10 mL ethanol and 2 mL of acetic acid. And then, the butyl titanate and tetraethyl orthosilicate were added to above mixed solution with the ratio of Si/Ti of 0.1 (molar ratio). After stirring for 4 h, the solution was put at 60 ℃ for 24 h to form the gel. The gel was calcinated at 500 ℃ for 9 h to obtain a TiO_2-SiO_2, which is marked as ST-W.

g-C_3N_4(CN) was obtained by calcination of

melamine in a muffle furnace at a rate of 5 °C/min to 520 °C and kept for 4 h.

g-C_3N_4/TiO_2-SiO_2 was obtained by ultrasonically dispersing a certain amount of g-C_3N_4 and TiO_2-SiO_2 in deionized water and followed by drying at 60 °C. Then the mixed materials were heated in a muffle furnace at a rate of 10 °C /min to 500 °C for 30 min. The mass ratio of g-C_3N_4 and TiO_2-SiO_2 of 1:10, 1:20 and 1:30 were marked as CN-10, CN-20 and CN-30, respectively.

2.2. Characterization

The phase composition was analyzed by an X-ray diffraction analyzer of Dmax Rapid II (Cu target, 0.154 nm, 40 kV, 40 mA, Rigaku Co.). The morphology was observed with a Quanta-450-FEG scanning electron microscope (FEI Co.). The degradation efficiency of the dye was measured by UV-2450 ultraviolet-visible spectrophotometer (Shimazu Co.). The specific surface area and pore size distribution of the samples were measured using a Gemini Vii 2390 (Micrometrics co.) analyzer.

2.3. Photocatalytic performance

The photocatalytic performance of the prepared samples was investigated by photocatalytic degradation methylene blue with a 500 W xenon illumination. The experiments were carried out in a photochemical reactor with a quartz jacket and cooled by circulating water. 15 mg of the prepared photocatalyst was added to 30 mL of methylene blue solution (2×10^{-5} mol/L) and stirred in the dark for 1 h to achieve the adsorption-desorption equilibrium. The concentration of the solution was measured every 15 minutes at 664 nm. The degradation rate is represented by C/C_0, where C_0 is the initial concentration of methylene blue solution, and C is the concentration of methylene blue solution at different degradation time.

3. Results and discussion

Fig. 1 shows the XRD pattern of the prepared samples. The XRD spectrum of ST-W has eight diffraction peaks at 2θ=25.28° (101), 37.80° (004), 48.05° (200), 53.89° (105), 55.06° (211), 62.69 ° (204), 70.31 ° (220), 75.03 ° (215), which is consistent with the anatase phase TiO_2 (PDF#21-1272). The CN has a diffraction peak at 2θ=27.86 ° (002), which coincides with the crystal plane of g-C_3N_4 (PDF#50-1512). It can also be seen that CN-10, CN-20 and CN-30 only exhibit characteristic peaks of anatase phase TiO_2 and g-C_3N_4. With the increase of g-C_3N_4 loading amount, the intensity of diffraction peak at 2θ=27.86 increase, however, there are no new diffraction peak appears, indicating that the doping of g-C_3N_4 did not change the crystal phase of the materials.

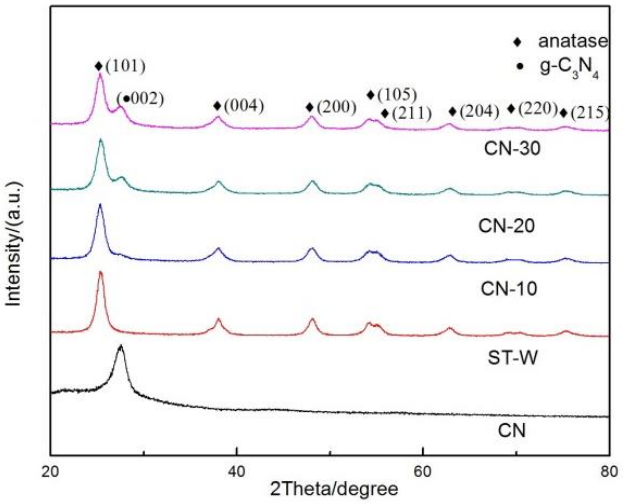

Fig. 1. XRD pattern of the prepared samples (color online)

Fig. 2 shows the SEM image of the prepared samples. It can be seen that g-C_3N_4 flakes are attached to the surface of TiO_2-SiO_2. With the increase of the amount of g-C_3N_4, the more g-C_3N_4 flakes can be observed. Fig. 3 shows the N_2 adsorption-desorption and pore size distribution curve of the prepared samples. All samples were type-IV isotherms and had an H1 hysteresis loop, indicating that the sample is a mesoporous material with a narrow pore size distribution. The pore properties of the prepared samples were shown in Table 1. It can be concluded that the specific surface area of the sample gradually decreases with the increase of the loading amount of g-C_3N_4. However, the pore size does not change much, indicating that no stacked pores are formed and the loaded g-C_3N_4 dispersed on the surface of the TiO_2-SiO_2 uniformly.

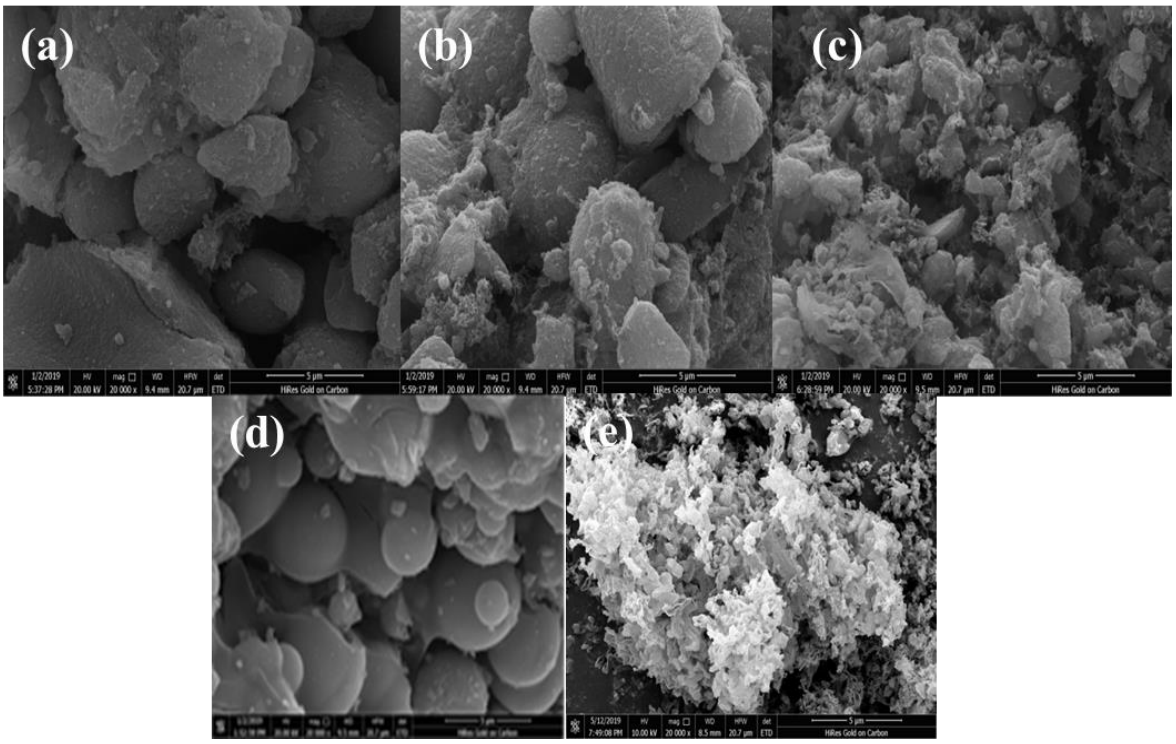

Fig. 2. SEM images of (a) CN-10 (b) CN-20 (c) CN-30 (d) ST-W (e) CN

Table 1. Pore properties of the prepared samples

Sample	Pore size/nm	Pore volume/(cm^3/g)	BET surface area/(m^2/g)
CN-10	13.22	0.4352	131.5
CN-20	13.35	0.4183	125.3
CN-30	13.50	0.4177	123.7
CN	2.97	0.1556	31.5
ST-W	13.36	0.4162	134.8

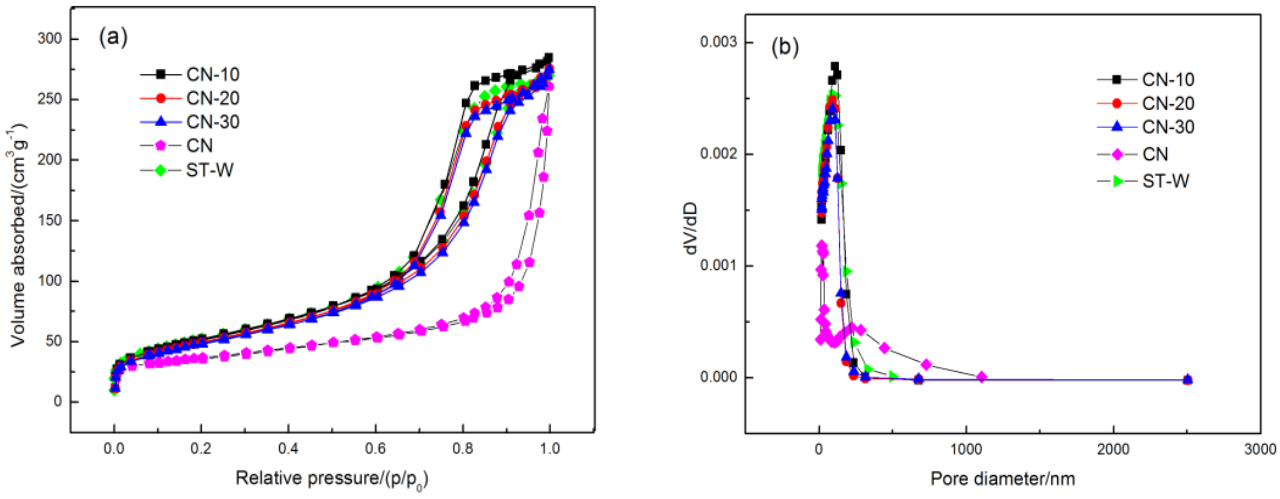

Fig. 3. (a) N_2 adsorption-desorption curve and (b) pore size distribution curve of the prepared samples (color online)

Fig. 4 displays the UV-vis DRS of the prepared samples. Compared with the absorption spectrum of ST-W, It can be seen from Fig. 4 that the ST-W absorbs almost exclusively in the ultraviolet region. As the g-C_3N_4 content increases, the absorption edges of the prepared samples extend to the visible light zone. Optical band gaps of all the samples were estimated using the Tauc relationship, $\alpha(h\nu)=A(h\nu\text{-}Eg)^{n/2}$, where α is the absorption coefficient, A is a constant, h is the Planck's constant, ν is the photon frequency, and Eg is the optical band gap [12]. For a direct transition semiconductor, n=1; for an indirect transition semiconductor, n=4. An extrapolation of the linear region of plot $(\alpha h\nu)^2$ vs $h\nu$ gives the value of the optical band gap, Eg, as shown in Fig. 4(b). The band gap of ST-W was calculated to be 3.20 eV, while those for CN, CN-10, CN-20 and CN-30 were valuated to be 2.87 eV, 3.17 eV, 3.11 eV and 3.00 eV, respectively.

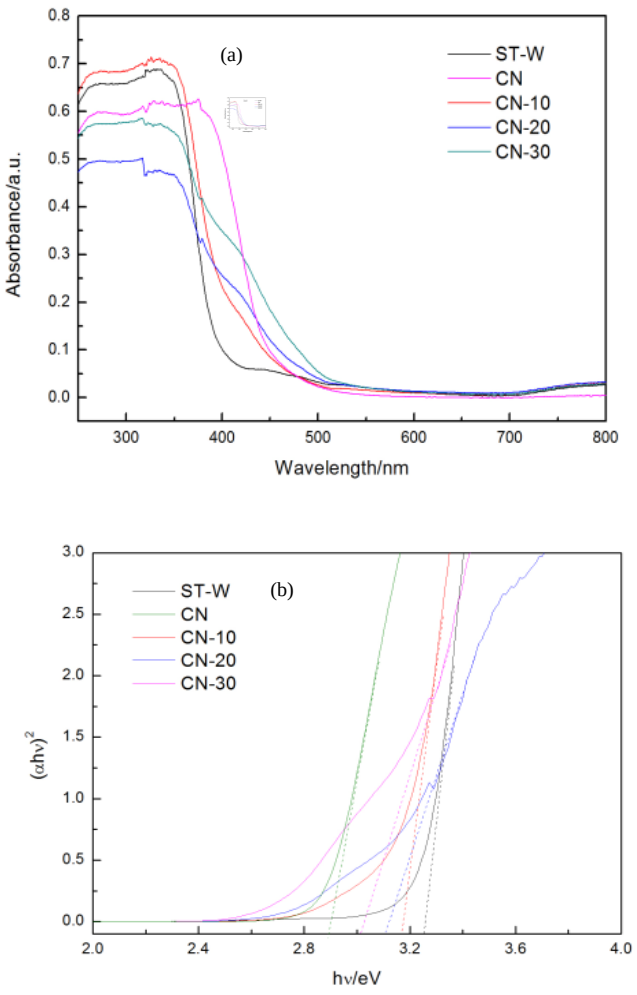

Fig. 4. (a) UV-vis spectrum and (b) optical band-gap energy Eg of the prepared samples (color online)

The photocatalytic activity of the prepared samples was investigated by degradation of MB simulated wastewater. As shown in Fig. 5 (a), after 60 min illumination, the MB has little degradation without the photocatalyst. When the prepared samples were added, the degradation rate of MB increased obviously. Among them, CN-20 has the best photocatalytic activity and fastest degradation rate (Fig. 5(b)), which can degrade nearly 100% MB. It can be seen that the mass ratio of g-C_3N_4 and TiO_2-SiO_2 plays an important role in the photocatalytic activity of the photocatalysts. The UV-visible absorption spectra of degrading MB by using CN-20 as a photocatalyst can be seen in Fig. 6.

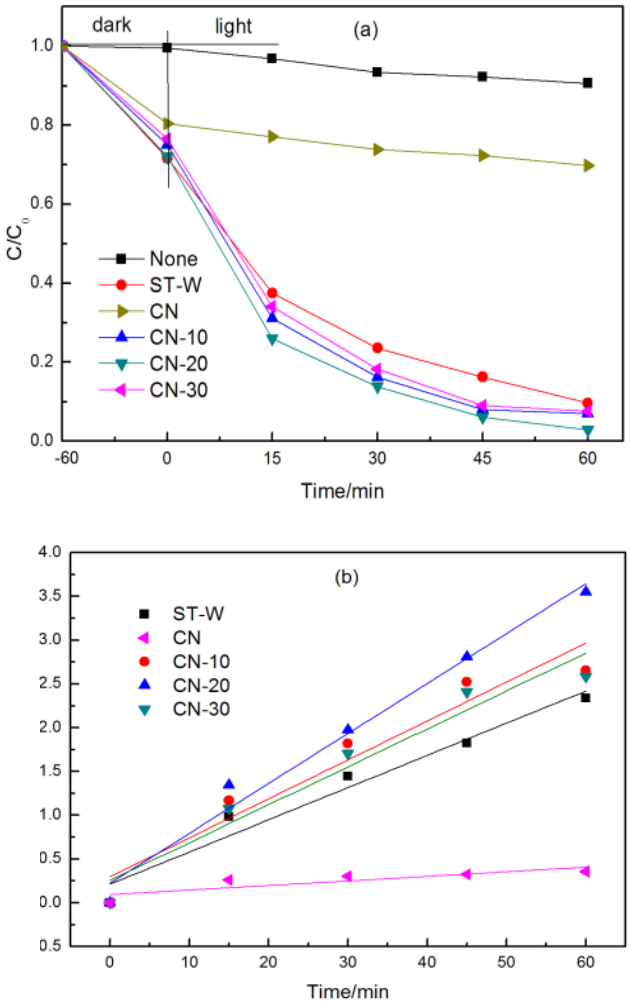

Fig. 5. (a) Photocatalytic degradation of MB and (b) First-order kinetic curve MB degradation by prepared samples (color online)

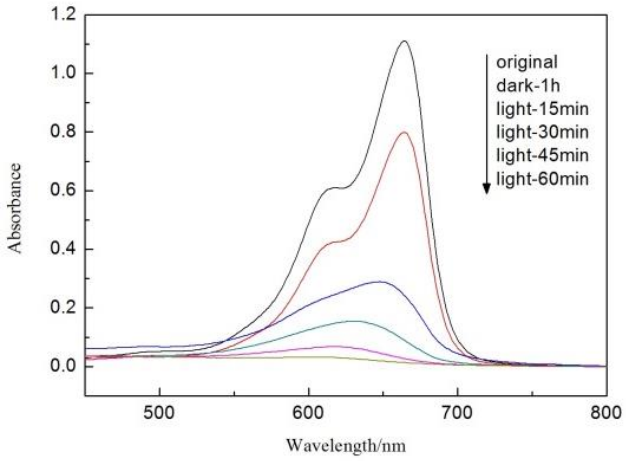

Fig. 6. Absorption spectrum of degradation process of MB (color online)

To investigate the photocatalytic activity of CN-20 further, the CN-20 was used to degrade the actual wastewater. The wastewater was taken from the domestic sewage of Xi'an Polytechnic University and used for photocatalytic experiments after pretreatment with microbial technology. Fig. 7 (a) is the absorption spectrum of actual wastewater after photocatalytic degradation at different time. The wastewater contains a wide variety of organic pollutants. It can be seen that the absorbance intensity decreased gradually as the illumination time increased. At the same time, the COD at different time was tested and the result was shown in Fig. 7 (b). The COD value of the wastewater reduced from 176 mg/L to 28.7 mg/L, indicating that organic pollutants in the wastewater were degraded during the photocatalytic process. The results indicate that the CN-20 has the potential application for actual wastewater purification.

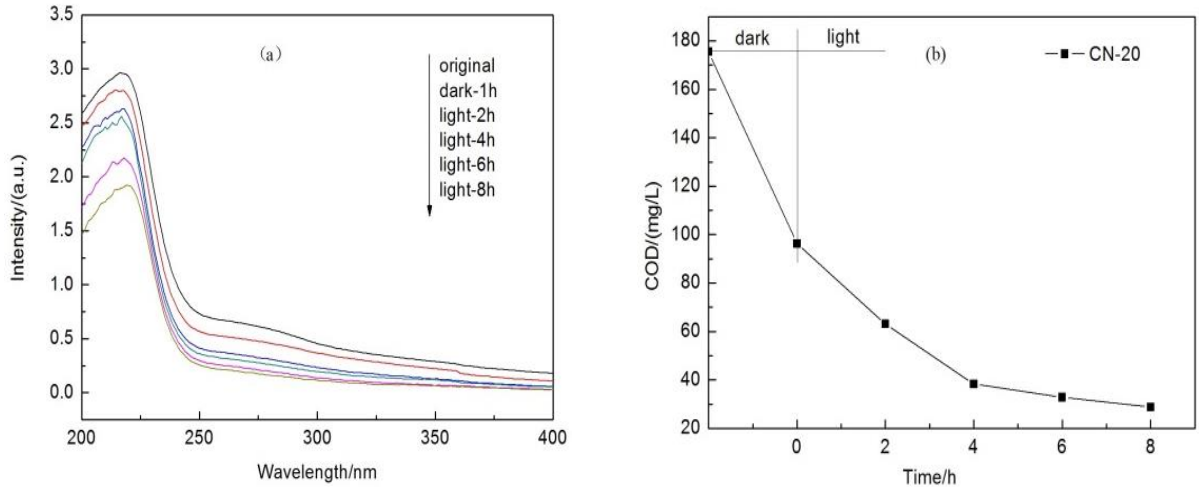

Fig. 7. (a) Absorption spectrum of actual wastewater (color online); (b) COD value over time

Considering the practical application, one of the important properties of the photocatalyst is its reuse stability. Therefore, the cycle experiment was performed. Fig. 8 shows the result for repeat utilization of CN-20 as the photocatalyst for MB degradation. The degradation efficiency of CN-20 remained above 80% after 5 times repeated use, indicating that CN-20 still has high photocatalytic activity after repeated use.

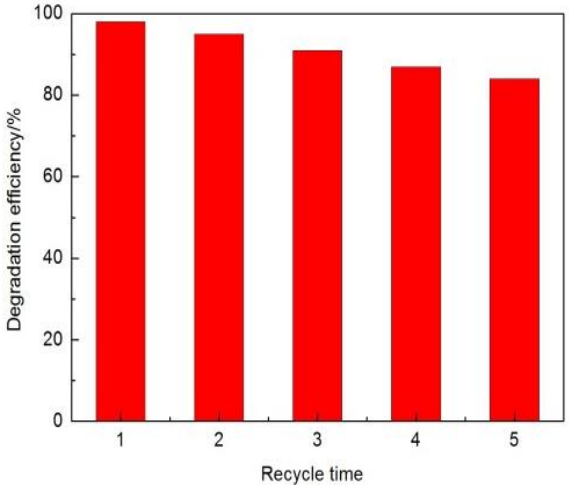

Fig. 8. Photocatalytic activity of the CN-20 for MB degradation with five times recycle uses (color online)

Photogenerated holes, superoxide radicals ($\cdot O^{2-}$) and hydroxyl radicals (·OH) are the main active species in the process of photocatalytic degradation of organic pollutants. In order to investigate the photocatalytic mechanism of the photocatalytic degradation progress, the disodium edetate (EDTA), p-benzoquinone (BQ) and tert-butanol (t-BuOH) were added to the MB solution to capture photogenerated holes, O^{2-} and ·OH, respectively. As shown in Fig. 9, the addition of the three capture agents can significantly decrease the MB degradation rate. Among them, the addition of t-BuOH has the obviously effect on the photocatalytic activity. It can be concluded that the main active species in the photocatalytic degradation of MB is the ·OH.

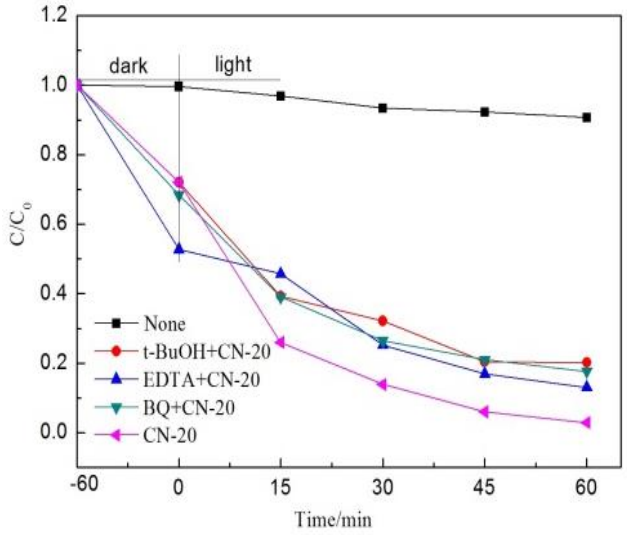

Fig. 9. Photo-generated carrier captured curve by photocatalytic degradation of MB by CN-20 (color online)

4. Conclusion

The g-C_3N_4/TiO_2-SiO_2 composite was successfully synthesized. The experimental results show that the photocatalytic activity of g-C_3N_4/TiO_2-SiO_2 is better than that of TiO_2-SiO_2. The optimal amount composition of g-C_3N_4 and TiO_2-SiO_2 can improve the photocatalytic activity of the composite. CN-20 can be used to reduce the COD value of actual wastewater effectively. The g-C_3N_4/TiO_2-SiO_2 material has good stability and reusability. The degradation rate of MB of CN-20 is more than 80% after 5 repeated use. The • OH produced in the photocatalytic process is the main active species for degrading MB. The results show that the g-C_3N_4/TiO_2-SiO_2 has great potential in photocatalytic degradation of dyeing wastewater.

Acknowledgements

This work is supported by the Science and Technology Department Research Funds of Shannxi Province, China (2021KW-12), Research and Development Program of Shaoxing Keqiao West-Tex Textile Industry Innovative Institute (19KQZD07) and National University Student Innovation Project (S202010709039).

References

[1] H. Mittal, S. M. Alhassan, S. S. Ray, J. Environ. Chem. Eng. **6**, 7119 (2018).
[2] J. Ambigadevi, P. S. Kumar, D. N. Vo, S. H. Haran, T. N. S. Raghavan, J. Environ. Chem. Eng. **9**, 104881 (2021).
[3] H. Dong, G. M. Zeng, L. Tang, C. Z. Fan, C. Zhang, X. X. He, Y. He, Water Res., **79**, 128 (2015).
[4] M. N. Chong, B. Jin, C.W. Chow, C. Saint, Water Res. **44**, 2997 (2010).
[5] Z. L. Yang, J. Lu, W. C. Ye, C. S. Yu, Y. L.Chang, Appl. Surf. Sci. **392**, 472 (2017).
[6] B. J. Sun, W. Zhou, H. Z. Li, L. P. Ren, P. Z. Qiao, F. Xiao, L. Wang, B. J. Jiang, H. G. Fu, Appl. Catal. B-Environ. **221**, 235 (2018).
[7] X. B. Chen, S. S. Mao, Chem. Rev. **107**, 2891 (2007).
[8] J. Tian, Y. H. Leng, Z. H. Zhao, Y. Xia, Y. H. Sang, P. Hao, J. Zhan, M. C. Li, H. Liu, Nano Energy **11**, 419 (2015).
[9] M. Z. Ge, Q. S. Li, C.Y. Cao, J. Y. Huang, S. H. Li, S. N. Zhang, Z. Chen, K. Q. Zhang, S. S. Al-Deyab, Y. K. Lai, Adv. Sci. **4**, 1600152 (2017).
[10] L. Zhang, W. Yu, C. Han, J. Guo, Q. H. Zhang, H. Y. Xie, Q. Shao, Z. G. Sun, Z. H Guo, J. Electrochem. Soc. **164**, H651 (2017).
[11] S. Protti, A. Albini, N. Serpone, Phys. Chem. Chem. Phys. **16**, 19790 (2014).
[12] S. G. Kumar, L. G. Devi, J. Phys. Chem. A **115**, 13211 (2011).
[13] W. K. Jo, T. S. Natarajan, Chem. Eng. J. **281**, 549 (2015).
[14] W. Chang, L. L. Yan, B. Liu, R. J. Sun, Ceram. Int. **43**, 5881 (2017).
[15] L. Zhang, D. W. Jing, X. L. She, D. J. Yang, Y. Lu, J. Li, Z. F. Zhen, L. J. Guo, J. Mater. Chem. A **2**, 2071 (2014).
[16] X. C. Wang, S. Blechert, M. Antonietti, ACS Catal. **2**, 1596 (2012).
[17] Y. T. Gong, M. M. Li, Y. Wang, ChemSusChem. **8**, 931 (2015).
[18] M. Majdoub, Z. Anfar, A. Amedlous, ACS Nano **14**, 12390 (2020).
[19] J. W. Fu, J. G. Yu, C. J. Jiang, B. Cheng, Adv. Energy Mater. **8**, 1701503 (2018).
[20] Y. Zheng, Z. H. Yu, H. H. Ou, A. M. Asiri, Y. L. Chen, X. C. Wang, Adv. Funct. Mater. **28**, 1705407

(2018).
[21] K. Sridharan, E. Jang, T. J. Park, Appl. Catal. B-Environ. **142**, 178 (2013).
[22] J. Shen, H. Yang, Q. Shen, Y. Feng, Q. Cai, CrystEngComm. **16**, 1868 (2014).
[23] Z. Tong, D. Yang, T. Xiao, Y. Tian, Z. Jiang, Chem. Eng. J. **260**, 117 (2015).
[24] Y. Y. Bu, Z.Y. Chen, Electrochim. Acta **144**, 42 (2014).
[25] L. B. Jiang, X. Z. Yuan, P. Yang, J. Liang, G. M. Zeng, Z. B. Wu, H. Wang, Appl. Catal. B-Environ. **217**, 388 (2017).
[26] F. Raziq, Y. Qu, X. Zhang, M. Humayun, J. Wu, A. Zada, H. Yu, X. Sun, L. Jing, J. Phys. Chem. C **120**, 98 (2016).
[27] L. Gu, J. Y. Wang, Z. J. Zou, X. J. Han, J. Hazard. Mater. **268**, 216 (2014).
[28] J. G. Yu, S. H. Wang, J. X. Low, W. Xiao, Phys. Chem. Chem. Phys. **15**, 16883 (2013).
[29] H. J. Yan, H. X. Yang, J. Alloy. Compd. **509**(4), L26 (2011).
[30] X. J. Wang, W. Y. Yang, F. T. Li, Y. B. Xue, R. H. Liu, Y. J. Hao, Ind. Eng. Chem. Res. **52**, 17140 (2013).

*Corresponding author: changwei72@163.com